Realization and Testing of the In Field Pointing Mechanism for the Evolved Laser Interferometer Space Antenna

Gert Witvoet* and Jet Human*

Abstract

An active tilt mirror mechanism, meant for correction of the constellation breathing of the evolved Laser Interferometer Space Antenna, has been designed and built. Its open-loop performance has been characterized in both the time and frequency domain. Based on this, a feedback controller has been designed and the resulting closed-loop performance has been assessed. Up to what is measurable in a normal lab environment, these experiments demonstrate compliance with the extreme pointing jitter requirement even when using the internal encoder as feedback sensor.

Introduction

The evolved Laser Interferometer Space Antenna (eLISA) mission, which is currently under development, is an ambitious project meant to accurately detect gravitational waves [1]. It will consist of three spacecraft flying in a triangular formation mutually 10^9 m apart in an Earth-like orbit around the sun, each carrying a free-flying proof mass. Detection of a passing gravitational wave requires measuring the distances between the proof masses with an accuracy of 10^{-11} m, which makes eLISA an extremely high sensitive instrument.

The eLISA mission still faces scientific and technological challenges to be solved before its tentative launch in 2034. One of which is constellation breathing, i.e., how to deal with slight variations in the angle between the interferometer arms over a period of a year due to orbital dynamics. In Telescope Pointing this is accounted for by rotating each of the six complete optical assemblies (two on each spacecraft). As a promising alternative, Airbus Defence & Space has developed the In-Field Pointing (IFP) concept [2], in which only a small tilt mirror, located in an intermediate pupil plane of the telescope, provides the means to steer the beam. IFP comes with a number of advantages over Telescope Pointing, such as actuation of a much smaller mass, possible smaller payload sizes, and possible simpler payload architectures [2, 3].

The feasibility of the IFP concept will be demonstrated in an experiment that Airbus DS is currently developing [3]. One of the critical components in this experiment is the In-Field Pointing Mechanism (IFPM), responsible for actuating the tilt mirror, on which there are high stability requirements. Built upon heritage with the Point-Ahead Angle Mechanism [4], which has similar stability requirements, TNO (Netherlands Organisation for Applied Scientific Research) has successfully carried out breadboard tests and made a design for this IFPM [5]. In this paper we will present the realized IFPM hardware, together with some important test results (in a normal laboratory environment). These tests include open-loop characterizations as well as closed-loop performance validations. Up to what is reasonably measurable in such a lab environment, the results show that the IFPM is indeed compliant with the requirements.

Hardware Design and Realization

The heart of the IFPM is a 50-mm flat tilt mirror, which needs to rotate ±2.5° in a whole year (equivalent to ±5° beam steering) to accommodate constellation breathing. In science mode it should do so with a maximum pointing jitter of just 5 nrad/√Hz over a large frequency range. This combination of large stroke

* TNO Technical Sciences, Delft, The Netherlands

and high accuracy requires the dynamic range of the IFPM to be in the order of 10^7 [2]. Moreover, the mirror is not allowed to introduce more than 3 pm/√Hz of optical path length (piston) noise.

Design concept

In the IFPM design, the rotation of the mirror is guided by two Haberland hinges, which are part of a single monolithic TiAlV structure. Their axis of rotation coincides with the mirror surface, in order to minimize the cross-coupling between the angular motion and optical path length variations. The mirror is connected to a translational actuator module via a stiff lever through the mirror rotation axis; this way the actuation force acts parallel to the mirror surface, which minimizes surface distortions.

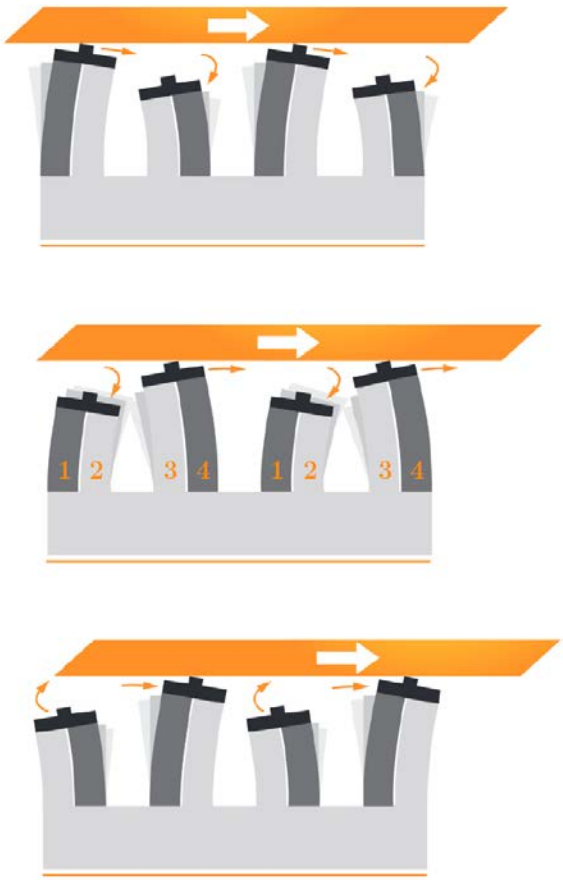

Figure 1. Operating principle of the walking piezo actuator. Due to the ellipsoidal movement of the tip of the legs, the ceramic rod moves in horizontal direction. The numbers indicate the phases; same-phase piezos are fed with the same voltage. Image courtesy of PiezoMotor®.

The actuation possibilities are limited for IFPM because of eLISA mission constraints (there are no electromagnetic forces allowed on the optical bench) and the large required stroke. After some successful breadboard tests [5], the Piezo LEGS walking actuator by PiezoMotor Uppsala AB has been selected. The operating principle of this walking piezo actuator is illustrated in Figure 1. Each actuator encompasses two sets of legs (depicted are two times two legs, the used piezostepper has two times three legs), where each leg consists of two pieces of piezoelectric material with a ceramic tip. By applying different voltages to each piezo the legs will elongate and bend. A proper choice of the four driving voltages (phases) can then cause an ellipsoidal movement of the tips of the legs, thereby creating a walking motion. As a result, a ceramic driving rod pushed against the legs with the right preload will move in the horizontal direction.

The piezostepper principle is friction-based and thus relatively stiff, while providing tens of newtons of holding force. The stroke is only limited by the length of the driving rod, and is thus principally infinite; the step size is only limited by the resolution of the DAC generating the voltages for the legs, and can thus be in the order of 0.1 nm or less (one actuator cycle is typically a few µm). As such, the complete IFPM assembly utilizes a hard actuator concept, which is both accurate, and stiff enough to potentially withstand launch loads.

Design improvements

The original IFPM design [5] had an actuator module in which three of such piezosteppers were combined in a triangular orientation, pushing against a triangular driving rod. The choice for three steppers was partly motivated by launch load and redundancy considerations, and partly to combine the guidance of the driving rod and preloading of the piezosteppers in one single component. This actuator module has been manufactured, but thorough testing showed that the nominal preload on the piezosteppers was too high and the distribution of the preload over the different legs was very uneven. It turned out that the performance of the actuator is very sensitive to such preload deficiencies, causing unreproducible irregular open-loop motion, which is why the original design never met its expected performance.

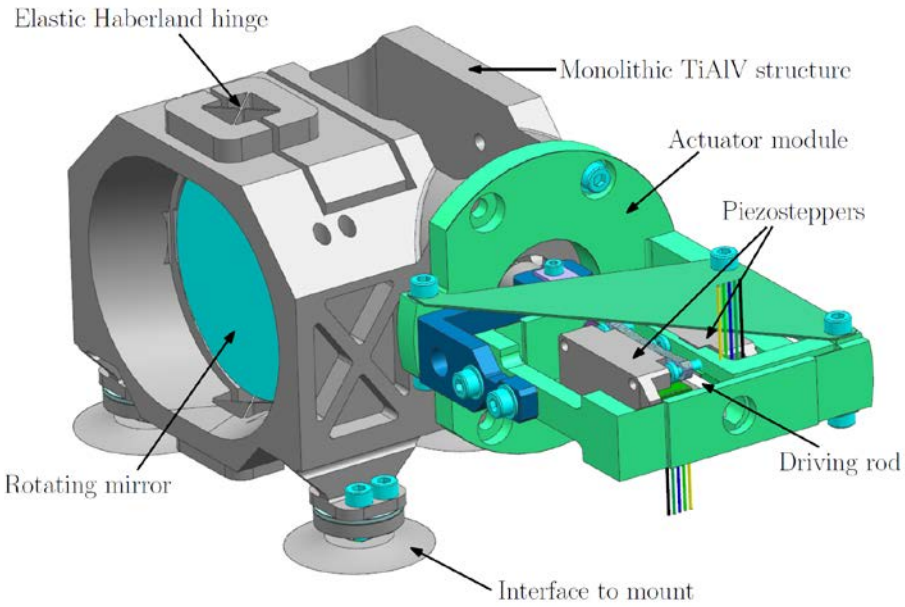

Figure 2. CAD model of the latest IFPM design.

It has therefore been decided to loosen the launch load and redundancy targets and focus on the proof-of-concept, by redesigning the actuator module to a two-stepper-concept. In this planar configuration, two piezosteppers are pushed on either side of a rectangular driving rod; the preload distribution along the legs is now much better defined and is tunable via the bolts through the leaf springs with which one of the piezosteppers is connected to the actuator module. Figure 2 shows a CAD model of the updated design.

Realization

The updated actuator module has been manufactured and assembled, and combined with the previously realized mirror unit. A picture of the complete IFPM assembly is shown in Figure 3. The setup has been tested under normal laboratory conditions (room temperature, atmospheric pressure), the results of which are presented in this paper. In these tests, the mirror rotation has been measured directly via a Renishaw differential interferometer. Both the reference and measurement beam are directed at the mirror; the mirror angle is calculated (with nrad resolution) using the distance between the beams and their optical path length difference. The mechanism is also equipped with a Micro-E incremental encoder and a 20-µm

pitch scale, located at a radius of 31.06 mm from the mirror rotation axis. This sensor has a 1.2-nm resolution, which is thus equivalent to 38.6 nrad of mirror rotation. The encoder was originally meant for beam acquisition purposes, but can also be used as a feedback sensor (as an alternative to the external interferometer).

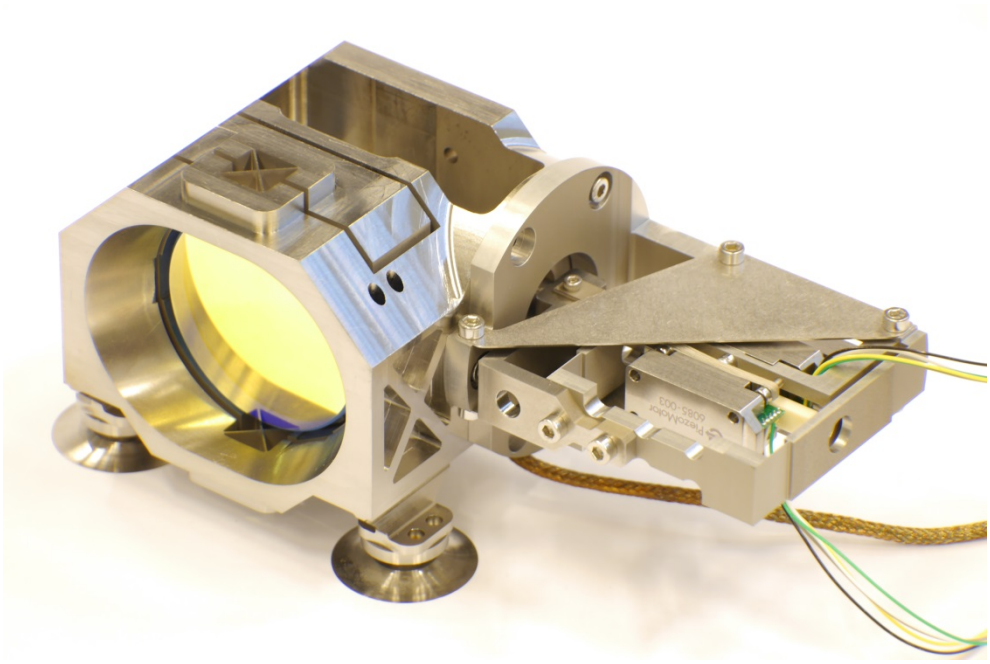

Figure 3. Picture of the realized two-stepper IFPM. (Photo: TNO / Gert Witvoet)

The piezosteppers are fed by four high-voltage space-qualified analog amplifiers, one for each of the four phases of the actuators. The voltage waveforms are generated by a dSpace data acquisition system with a 16-bit D/A converter; the encoder (via a 24-bit digital encoder interface) and the interferometer (via a 16-bit A/D converter) are connected to the same dSpace system. This system offers a rapid prototyping environment in MATLAB/Simulink, which provides great flexibility in measurement possibilities and controller design.

System Behavior

The motion of the legs of the walking actuator is determined by the voltage distribution along the four phases as a function of time. Although the open-loop motion will never be perfectly linear, the exact shape of these voltage waveforms has a large influence on the velocity variations during an actuator cycle [6]. For example, the horizontal and vertical motion of the first set of legs can be approximated by

$$x_{p1} = c_1\big(u_1(t) - u_2(t)\big)$$
$$y_{p1} = c_2(u_1(t) + u_2(t))$$

where c_1 and c_2 are motor coefficients and $u_1(t)$ and $u_2(t)$ are the voltages applied to phase 1 and 2 respectively [7]. Pure sinusoidal waveforms are known to exhibit zero velocity at the transfer points (i.e., when one set of legs take over from the other), which is undesirable from a performance point-of-view. Therefore so-called asymmetric waveforms [7] have been used, where the voltage of the first phase is defined between 0 and the maximum A (here 48 V) as

$$u_1(t) = \begin{cases} \frac{1}{2}A + \frac{1}{2}A\sin\left(2\pi\frac{\alpha(t)}{2q}\right), & \alpha(t) \in [0, q] \\ \frac{1}{2}A + \frac{1}{2}A\sin\left(2\pi\frac{\alpha(t)-1}{2(1-q)}\right), & \alpha(t) \in [q, 1], \end{cases}$$

and the other three phases are shifted 90°, 180° and 270°. The actuator phase $\alpha(t)$ denotes a specific moment in the waveform cycle, and $0 < q < 1$ is the asymmetry factor where $q = 0.5$ is a pure sine wave. After some open-loop testing, $q = 0.6$ has been chosen, since this value returned the smallest velocity variations during a complete waveform cycle.

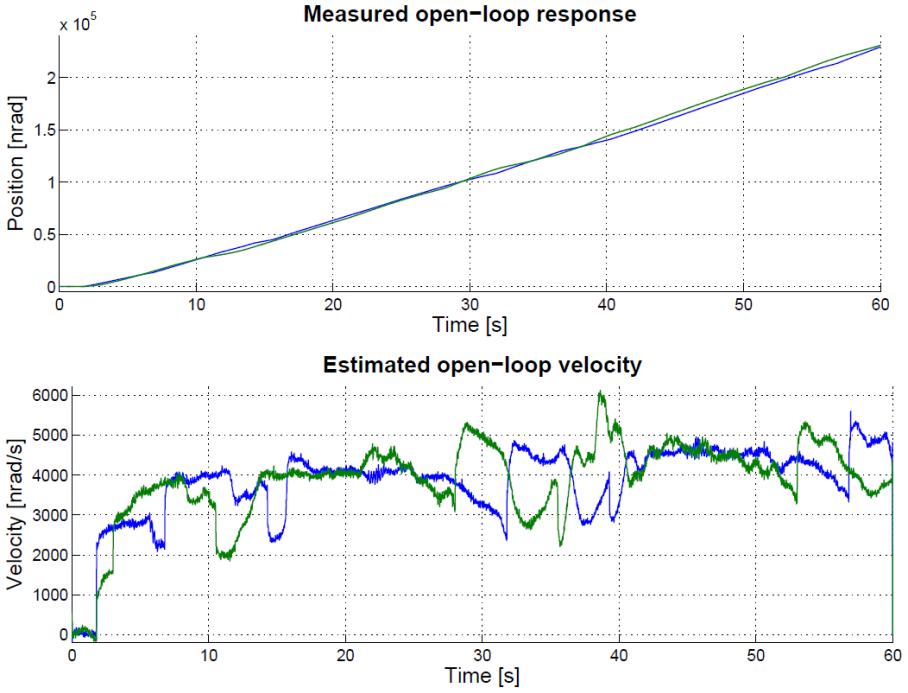

Figure 4. Measured open-loop mirror rotation and its estimated velocity using a constant 0.02-Hz waveform frequency.

Two specific open-loop results using these waveforms are shown in Figure 4, depicting the mirror rotation measured by the interferometer and the derived velocity estimate. Both experiments use a constant frequency of 0.02 Hz, i.e. the actuator phase $\alpha(t)$(t) increases linearly, so that a complete cycle takes 50 s. Indeed, the mirror rotation is not perfectly linear, but the bottom plot shows that there are no stick-slip effects or reversed directions, which would be show-stoppers for accurate long-stroke closed-loop motion. The velocity variations are at most a factor 3, which are relative easy to account for in a controller design.

Frequency response function measurements

Further characterization of the IFPM behavior has been done in the frequency domain, via local frequency response function (FRF) measurements around various actuator operating points [8]. To this end the waveforms have been set at different nominal $\alpha_{\mathrm{nom},k}$, around which a small amount of additional noise $\bar{\alpha}(t)$ has been added, which results in a mirror response y. The local dynamics around operating point k can then be calculated as the ratio between the cross-power density $S_{y\bar{\alpha}}$ and auto-power density $S_{\bar{\alpha}\bar{\alpha}}$ of the two signals

$$H_k(j\omega) = \frac{S_{y\bar{\alpha}}(j\omega)}{S_{\bar{\alpha}\bar{\alpha}}(j\omega)}.$$

The resulting FRFs for 21 different nominal phases $\alpha_{\mathrm{nom},k}$ along a full actuator cycle are shown in Figure 5, using either the interferometer or the encoder as sensor for y (notice the gain difference between the two, since one is expressed in nrad and the other in nm). The latter obviously has a worse coherence and is noisier, since it has a much coarser resolution than the interferometer. Apart from that, both results are very much alike. All FRFs show the same resonances and more or less the same anti-resonances, which implies that the dynamics is nearly constant over a full actuator cycle. The FRFs only differ in their gain, which is particularly clear for low frequencies. These local DC-gain variations of at most 9 dB can directly be linked to the observed velocity variations in Figure 4, since this is roughly a factor 3. Moreover, all FRFs have the same low-frequent phase, which confirms that there are no direction reversals.

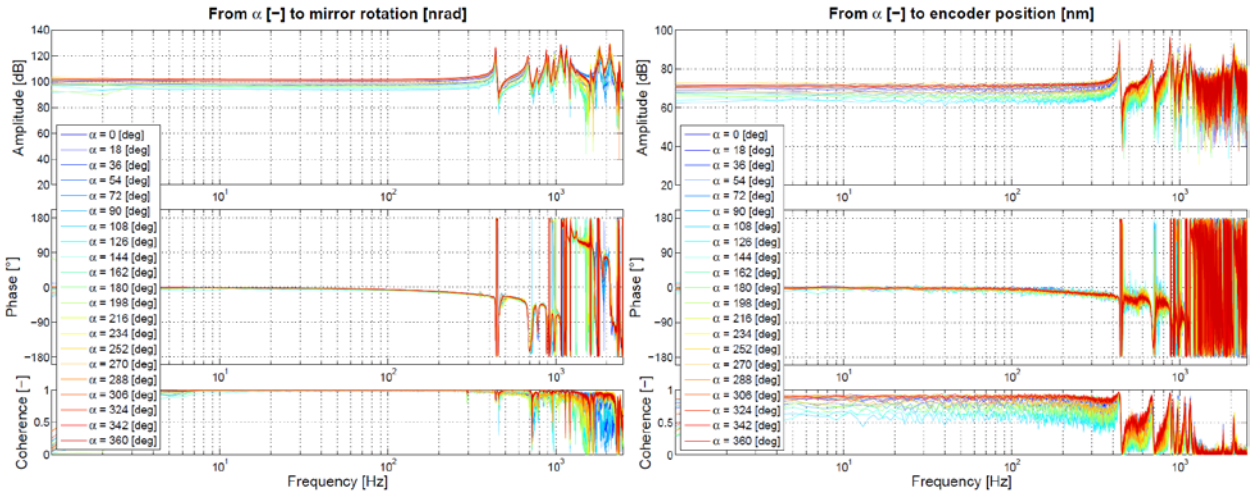

(a) Using the interferometer as sensor

(b) Using the internal Micro-E encoder as sensor

Figure 5. Measured FRFs as a function of the actuator phase α.
Note that 360° is equivalent to $\alpha_{\mathrm{nom}} = 1$.

Closed-Loop Performance

The friction-based Piezo LEGS actuators are not meant to provide accurate open-loop motion, which is indeed confirmed by the above measurements. Hence, to meet the extreme accuracy requirements, the IFPM has to be operated in closed loop.

Controller design

Since the DC-gain variations along the actuator cycle are relatively small, a fixed linear controller can be sufficient to demonstrate the IFPM performance. The foreseen feedback loop is illustrated in Figure 6, where the proposed controller structure encompasses

- a double integrator to allow perfect tracking of linearly increasing setpoints;
- a zero to create phase-lead around the cross-over frequency (i.e. for closed-loop stability);
- a second-order low-pass filter to suppress higher-order dynamics.

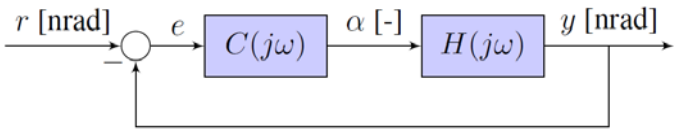

Figure 6. Feedback loop for controlling the mirror angle $y(t)$ via the actuator phase $\alpha(t)$.

The controller parameters have been tuned specifically on the measured FRFs in Figure 5(a), i.e., based on the high-resolution interferometer measurements. The parameters have been chosen such that all local FRFs yield a robustly stable closed loop with a high as possible bandwidth. In this case the robustness has been defined by both a maximum phase margin of 55° and a modulus margin (maximum value of the closed-loop sensitivity function) of at most 3.5 dB. The resulting open loops $H_k(j\omega)C(j\omega)$ are depicted in Figure 7, both as a Bode and a Nyquist diagram. The latter shows that the closed loop is indeed stable for all local FRFs, since all curves are on the right side of the point (-1,0) [9]. Moreover, all loops indeed satisfy the set modulus margin (black circle) and phase margin (black arc). Figure 7(a) shows that the achieved bandwidth lies between 26 and 62 Hz.

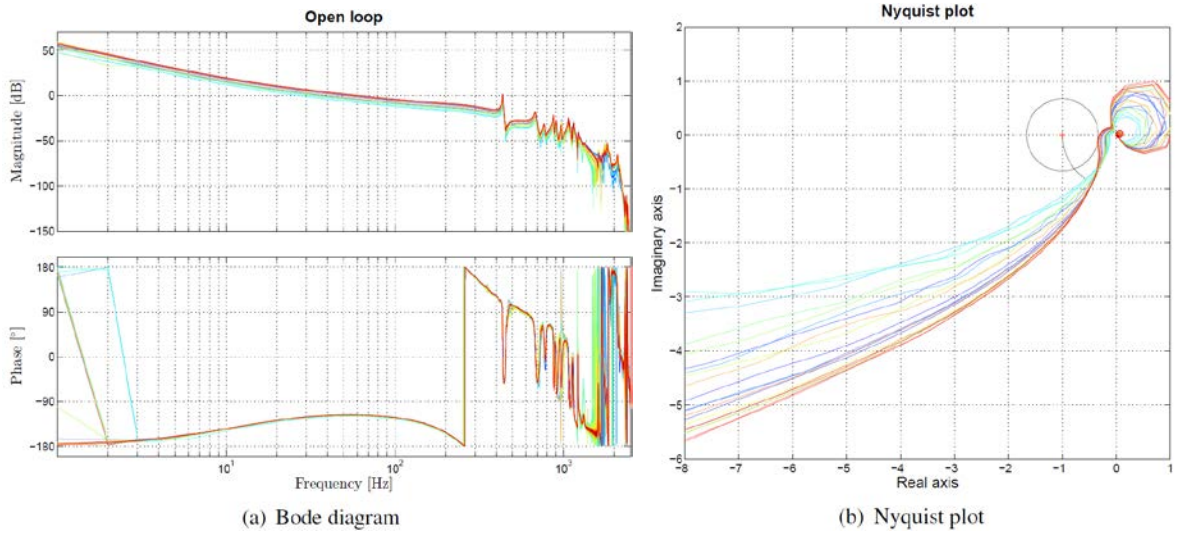

(a) Bode diagram (b) Nyquist plot

Figure 7. Frequency domain representations of the open loop $H_k(j\omega)C(j\omega)$.

Measured tracking performance

The designed feedback controller has been implemented in the Simulink / dSpace environment, and used to validate the IFPM performance. As was originally the intention, first the external interferometer been selected as feedback sensor.

Figure 8 shows the results in terms of the amplitude spectral density (ASD) of the closed-loop error during various different experiments. The dashed line indicates the 5 nrad/√Hz pointing jitter requirement. During these experiments both forward and backward movements has been carried out with three different velocities ranging from 12.5 nrad/s (specified science mode velocity) to 2250 nrad/s. Strictly speaking the performance does not have to be demonstrated for velocities larger than 12.5 nrad/s, but these are included anyway to demonstrate the IFPM behavior over a larger stroke where the piezosteppers go through a number of cycles. Clearly the requirement is met over all frequencies in all closed-loop experiments.

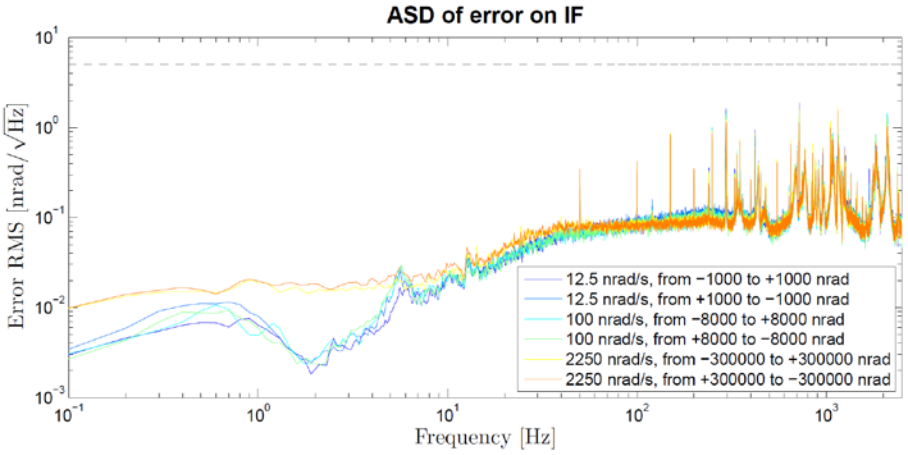

Figure 8. Measured amplitude spectral density (ASD) of the closed-loop error using the interferometer as feedback sensor.

However, interferometer measurements are known to be very sensitive to items such as temperature variations and turbulence, which usually results in low-frequency drifts. Hence, when the interferometer is used as feedback sensor, the mirror rotation is actually tracking these drifts. As an alternative, it has therefore been decided to try to close the loop on the Micro-E encoder and use the interferometer as a reference sensor. Since Figure 5 showed that the dynamics are the same for both sensors, the same controller as discussed above can be used for this purpose (only an additional gain of 1/0.03106 had to be included to convert the encoder nm-readout to nrad).

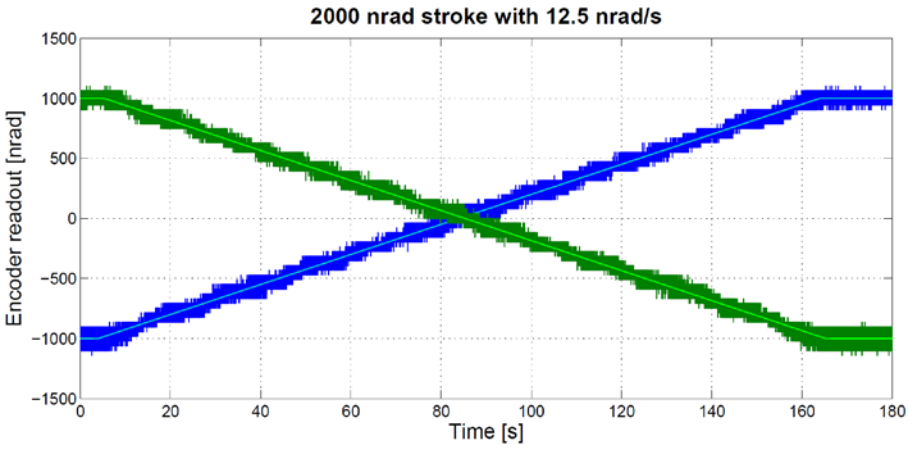

Figure 9. Two closed-loop responses with 12:5 nrad/s mirror rotation (science mode) using the internal encoder as feedback sensor. The setpoints are drawn on top of the measured rotations.

Two specific closed-loop time responses using this approach are depicted in Figure 9. In these experiments the setpoint is changing with the science mode velocity, both forward and backward, which the encoder is tracking successfully. The encoder resolution steps are clearly visible in the response.

The effect of these steps on the ASD of the error (as measured by the encoder) is however very limited, as is shown in Figure 10(a). Due to the coarser resolution, the level of the ASD is much higher than in Figure 8, but still the requirement is met quite easily, both for the science-mode and the large-stroke scenario. This implies that IFPM can be used with high accuracy in a stand-alone configuration, i.e.

independent of any external metrology, which is very beneficial in the current breadboarding phase of the IFP project.

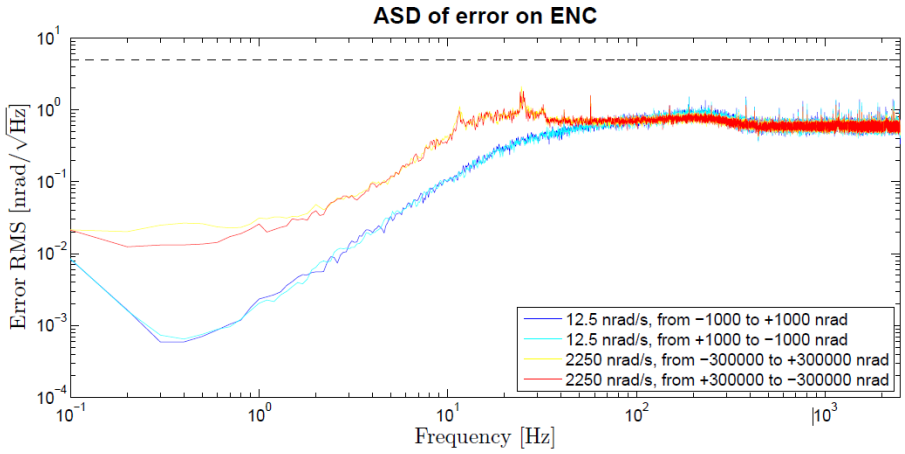

(a) As measured by the encoder

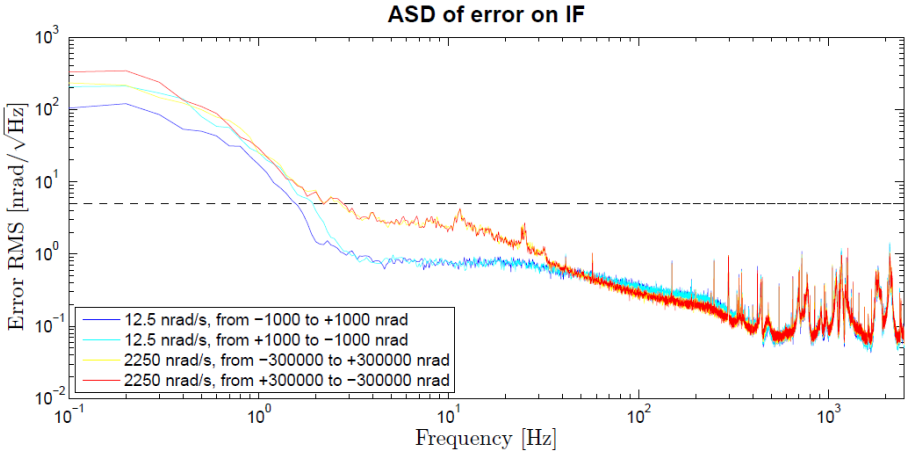

(b) As measured by the interferometer

Figure 10. Amplitude spectral densities of the closed-loop error using the internal encoder as feedback sensor.

Notice that the shape of the ASD in Figure 10(a) (especially for the 12:5 nrad/s case) resembles the designed closed-loop sensitivity function

$$S(j\omega) = \frac{1}{1 + H(j\omega)C(j\omega)}$$

which is typically small for low frequencies and constant for high frequencies. In the transition between these two regions the bandwidth can be estimated, which is indeed in the order of 30 Hz.

Figure 10(b) shows the ASD of the interferometer readout for the same experiments. This plot shows a violation of the requirement below 2 Hz. As pointed out before, this could partly be attributed to drift in the reference sensor itself, which is difficult to rule out in a normal unconditioned laboratory environment. As such, we can conclude that the IFPM performs compliant, at least up to what can be measured in a

normal lab. The IFPM performance for very low frequencies will therefore be validated in future environmental tests to be carried out by Airbus DS in their IFP breadboard setup.

Conclusions

In this paper we have presented the design and realization of the In-Field Pointing Mechanism for the eLISA mission. This mechanism encompasses a tilt mirror guided by Haberland hinges, which is actuated by walking piezo actuators. The redesign of the actuator unit to a planar configuration has improved the open-loop behavior significantly, resulting in local velocity variations of just a factor 3 and nearly constant dynamics over a full actuator cycle.

The open-loop measurements have been taken into account in a robust high-performance controller design. This controller has been combined with both interferometer and encoder feedback; the latter has demonstrated that IFPM can be operated stand-alone with high accuracy. In both cases the resulting ASDs suggest compliance with the maximum allowed pointing jitter.

However, in our unconditioned laboratory the performance could only be guaranteed for frequencies above 2 Hz. For a real validation of the low-frequent performance a better conditioned environment is required. This validation will be carried out by Airbus DS in their environmental tests. In these tests the piston jitter of the IFPM will also be assessed.

Acknowledgments

The authors would like to thank Dennis Weise, Ewan Fitzsimons and Christina Brugger (Airbus Defence & Space) for the fruitful collaboration within the IFPM project, Per Bendixen (Piezomotor) for his help on improving the actuator module, and former colleagues Joep Pijnenburg, Niek Rijnveld and Martijn te Voert for their contributions to the IFPM development.

References

[1] K. Danzmann, “LISA mission overview,” *Advances in Space Research*, vol. 25, no. 6, pp. 1129–1136, 2000.

[2] D. R. Weise, P. Marenaci, P. Weimer, H. R. Schulte, P. Gath, and U. Johann, “Alternative opto-mechanical architectures for the LISA instrument,” *Journal of Physics: Conference Series*, vol. 154, no. 1, p. 012029, 2009.

[3] C. Brugger, B. Broll, E. Fitzsimons, U. Johann, W. Jonker, S. Lucarelli, S. Nikolov, M. te Voert, D. Weise, and G. Witvoet, “An experiment to test in-field pointing for LISA,” in *Proc. 10th ICSO*, Tenerife, Spain, October 2014.

[4] N. Rijnveld and J. Pijnenburg, “Picometer stable scan mechanism for gravitational wave detection in space,” *Proc. SPIE*, vol. 7734, p. 77341R, 2010.

[5] J. Pijnenburg, N. Rijnveld, and H. Hogenhuis, “Extremely stable piezo mechanisms for the new gravitational wave observatory,” *Proc. SPIE*, vol. 8450, p. 84500C, 2012.

[6] R. Merry, M. Maassen, M. van de Molengraft, N. van de Wouw, and M. Steinbuch, “Modeling and waveform optimization of a nano-motion piezo stage,” *IEEE/ASME Trans. Mechatronics*, vol. 16, no. 4, pp. 615–626, 2011.

[7] R. Merry, N. de Kleijn, M. van de Molengraft, and M. Steinbuch, “Using a walking piezo actuator to drive and control a high-precision stage,” *IEEE/ASME Trans. Mechatronics*, vol. 14, no. 1, pp. 21–31, 2009.

[8] R. Merry, J. Holierhoek, M. van de Molengraft, and M. Steinbuch, “Gain scheduling control of a walking piezo actuator,” *IEEE/ASME Trans. Mechatronics*, vol. 19, no. 3, pp. 954–962, 2014.

[9] S. Skogestad and I. Postlethwaite, *Multivariable Feedback Control: analysis and design*. Chichester, UK: John Wiley, 2005.